Nanoscale

Radio Frequency Heating of Metallic and Semiconducting Single-Walled Carbon Nanotubes

Journal:	*Nanoscale*
Manuscript ID	NR-ART-02-2019-001600.R1
Article Type:	Paper
Date Submitted by the Author:	01-May-2019
Complete List of Authors:	Anas, Muhammad; Texas A and M University System, Chemical Engineering Zhao, Yang; University of Florida, Chemical Engineering Saed, Mohammad; Texas Tech University, Department of Electrical and Computer Engineering Ziegler, Kirk; University of Florida, Department of Chemical Engineering Green, Micah; Texas Tech University, Chemical Engineering; Texas A and M University System, Chemical Engineering

Radio Frequency Heating of Metallic and Semiconducting Single-Walled Carbon Nanotubes

Muhammad Anas[1], Yang Zhao†[2], Mohammad A. Saed[3], Kirk J. Ziegler[2,4], Micah J. Green[*1,5]

[1] Artie McFerrin Department of Chemical Engineering, Texas A&M University, College Station, TX, USA

[2] Department of Chemical Engineering, University of Florida, Gainesville, FL, USA

[3] Department of Electrical and Computer Engineering, Texas Tech University, Lubbock, TX, USA

[4] Department of Materials Science & Engineering, University of Florida, Gainesville, FL, USA

[5] Department of Materials Science & Engineering, Texas A&M University, College Station, TX, USA

Current address: † Postdoctoral Researcher, University of Pennsylvania, Department of Chemical and Biomolecular Engineering, Philadelphia, PA 19104, USA

[*]Corresponding author, email: micah.green@tamu.edu

Abstract

Here we report the effect of metallic (m-) and semiconducting (s-) properties of single-walled carbon nanotubes (SWCNTs) on the response of SWCNT films to radio frequency (RF) heating. We separated high-purity m- and s-SWCNTs from an initial SWCNTs mixture and prepared thin films using vacuum filtration method. The areal density of the films is 9.6 μg/cm^2, and the DC conductivities are in the range of 7,800-49,000 S/m. We show rapid and non-contact Joule heating of films using a fringing-field RF applicator, and we observe maximum heating rates in the frequency range of 60-70 MHz. We determine that the more conductive m-SWCNT films reflect RF fields and heat at a maximum rate of 1.51 °C/s compared to maximum heating rate of 25.6 °C/s for s-SWCNT films. However, m-SWCNTs heat up faster than s-SWCNTs when dispersed in a dielectric medium. Our results confirm the non-monotonic relationship between RF heating rate and conductivity for CNT-based materials such that conductivity is required for heating but high values are correlated with reflections. Our findings also suggest that RF heating could be a possible metric for evaluating film purity because impurities in the films affect the conductivity and thus RF heating rate. We anticipate that RF heating may occur in SWCNT-based electronics and affect their performance.

Introduction

Carbon Nanotubes (CNTs) possess exceptional properties such as high strength, thermal conductivity, and electrical conductivity which have led to their widespread use in advanced composites (1, 2), energy storage devices (3, 4), filtration membranes (5, 6), multifunctional fabrics (7, 8), and most importantly high-performance electronics (9-11).

Single-walled carbon nanotubes (SWCNTs) have tunable electronic properties which make them far more valuable in high-performance electronics compared to their multi-walled analogues (12-15). If a SWCNT is conceived as a rolled-up sheet of graphene, then the rolling direction is defined by chirality. Depending on this chirality, the electronic band structure of SWCNTs can be either metallic (m-) or semiconducting (s-) (16-18).

The typical synthesis of SWCNTs results in a complex mixture of m- and s-SWCNTs but many methods have already been developed to separate these fractions (19-22). The successful purification of m- and s-SWCNTs has expanded their applications to nanoelectronics (15, 23, 24). The m-SWCNTs could be used as interconnects allowing higher current densities than copper and aluminum (25, 26). The s-SWCNTs with tunable energy bandgaps could offer miniaturization of electronic devices such as transistors and sensors (13, 27-30). Although there has been interest in fabricating devices that use individual SWCNT as components, SWCNT films are preferred in electronics as an alternative configuration to directly-grown individual SWCNTs due to their ease of fabrication and reproducible characteristics (9, 31-35). For example, s-SWCNT films have already been used in thermoelectric devices (36), field effect transistors (FETs) (37, 38), and diodes (23, 39). Additionally, thin films of m-SWCNT and s-SWCNT can be applied as conductive coatings in photovoltaics (40), electrochromic devices (41), and flat panel displays (42, 43).

All these SWCNT-based devices are either used in circuits for radio frequency (RF) applications or could possibly interact with electric fields (E-field) at RF frequencies during operation (24, 44). Therefore, it is of great importance to probe the interaction of m- and s-SWCNTs with RF fields since these interactions are not well understood. Prior work on this front is mostly focused on dilute SWCNT dispersions, particularly in medical applications (45, 46). For example, Gannon *et al.* (45) used RF energy to induce heating in aqueous SWCNT samples. They injected 500 mg/L mixed SWCNTs suspension into rabbit tissues and applied RF power of 600 W at 13.56 MHz to heat the suspension at 8 °C/s. This locally-induced heating of SWCNTs successfully destroyed the tumor cells. The only study that differentiates the response of m-SWCNT and s-SWCNT when exposed to RF fields is by Corr *et al.* (46). In this study, the interaction of RF fields with 95% pure m-SWCNT and 95% pure s-SWCNT dispersions was investigated at the operating frequency of 13.56 MHz. It was reported that 100 mg/L dispersions of m- and s-SWCNT heated at 0.20 °C/s and 0.35 °C/s, respectively, at RF

power of 500 W. The same study also stated that the presence of a conductive host such as NaCl in dispersions did not enhance the heating rate but rather diminished the electric fields near m- and s-SWCNTs.

Recently, our group has shown that multi-walled carbon nanotube (MWCNT)-loaded polymer composites can directly couple with electric fields at RF frequencies (1-200 MHz) and rapidly heat via Joule heating. We demonstrated different RF electric field applicator configurations such as direct-contact, parallel plate, and interdigitated fringing-field for heating MWCNT-loaded composites. We observed heating rates of 16 °C/s for 5 wt.% MWCNT composites at RF power as low as 10 W (47). Our RF heating technique cured thermosets faster compared to conventional oven-based curing due to localized volumetric heating. We also applied our technique to rapidly cure thermoset adhesives in metal-metal bonding and assembled an automotive structure. These findings also have applications to curing of thermoset adhesives in plastic-plastic bonding and welding of 3D-printed plastic structures (48). However, it is not yet understood how m- and s-SWCNTs would behave in the context of RF heating. Delineating how these SWCNTs differ would aid in understanding the effect of m- and s-shells in MWCNTs as well.

In this work, we investigate the heating response of m- and s-SWCNT films to applied RF energy. We successfully separate high-purity m- and s-SWCNTs fractions from an initial SWCNTs mixture and fabricate thin films of low areal densities. We measure electrical properties of the films and use a fringing-field RF applicator to heat the films. We show rapid and non-contact coupling of RF electrical fields with the films and observe heating with high heating rates. We find that RF heating rate scales inversely with the bulk DC conductivity of the film. The more conductive m-SWCNT films reflect RF fields and heat at lower rates compared to s-SWCNT films. We also observe that the presence of impurities lowers the overall conductivity of m-SWCNT films, which significantly increases the heating rate. Our findings suggest that RF heating could be used as a metric for film purity, and that RF heating may occur in SWCNT-based electronics.

Results and Discussion

We obtained high-purity m- and s-SWCNTs by first injecting an initial SWCNT dispersion into a Sepharose hydrogel-packed chromatography column, and then separating the fractions through elution with different surfactant solutions. Figure S1 shows the diameter distribution of initial SWCNT dispersion. The m-SWCNTs were collected first through elution with 1 wt. % aqueous SDS solution and concentrated to 5.10 ppm. A small fraction of m-SWCNTs was also obtained after SDS to DOC surfactant exchange process and concentrated to 2.71 ppm. Finally, the s-SWCNTs were collected through elution with 1 wt. % aqueous DOC solution and concentrated to

11.7 ppm. Figure S2 shows images of initial SWCNT dispersion, m-SWCNT SDS-based dispersion, and s-SWCNT DOC-based dispersion. The differences between these samples is clearly noticed from different colors. The initial SWCNT dispersion has a black color, the separated m-SWCNT dispersion has a red color, and the s-SWCNT dispersion has a green color. Figure 1 shows the normalized absorption spectra of s-SWCNTs dispersed in aqueous DOC solution, and m-SWCNTs dispersed in aqueous DOC and SDS solutions, respectively. The absorption in the S_{11} and S_{22} bands of s-SWCNTs dispersed in DOC solution indicates that this SWCNT dispersion contains major s-SWCNT species. This is because the regions labeled S_{11} and S_{22} correspond to excitonic absorption bands of s-SWCNTs due to first and second one-dimensional van Hove singularities (vHS), respectively (49). In addition, fluorescence spectra (Figure S3) further confirms the presence of different s-SWCNT species in the dispersion. On the other hand, the absorption in the M_{11} band of m-SWCNTs dispersed in DOC and SDS solutions indicates that these SWCNT dispersions are concentrated with m-SWCNTs because the M_{11} region corresponds to the absorption band of m-SWCNTs (49). Moreover, the fact that m-SWCNTs do not fluoresce (Figures S4-S5) but absorb in the M_{11} band is also a strong proof of their high purity in the dispersions. The purities of dispersions were calculated based on areas of the M_{11} and S_{22} bands. The s-SWCNT dispersion purity is nearly 100% while the m-SWCNT dispersions have purities of around 90-98%. The purity can be further increased by using higher concentration of initial SWCNTs dispersion and selecting other high-throughput hydrogels such as Sephacryl 100 HR or 200 HR for separation (50, 51). Note that the absorption peaks due to s-SWCNT impurities are also observed for the DOC-based dispersion of m-SWCNTs.

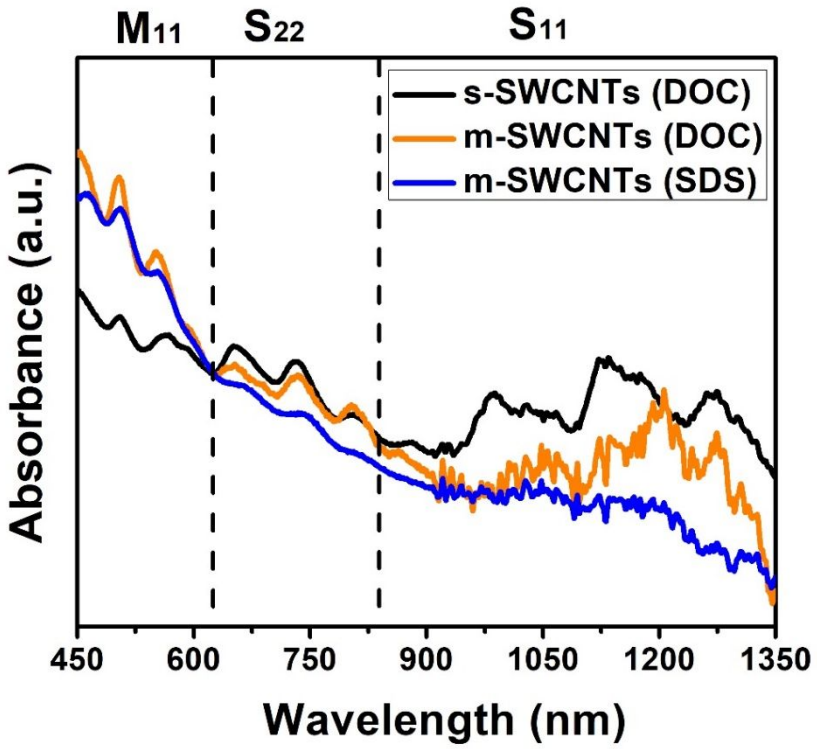

Figure 1. Normalized absorbance spectra (λ = 626 nm) of 11.7 ppm s-SWCNTs dispersed in DOC solution, 2.71 ppm m-SWCNTs dispersed in DOC solution, and 5.10 ppm m-SWCNTs dispersed in SDS solution.

We vacuum filtered m- and s-SWCNT dispersions through a 0.1 μm pore size alumina membrane to make 200 nm thin films with the areal density of 9.6 μg/cm^2. It is also possible to make films using other more efficient techniques such as ultrasonic spraying of CNT dispersions (36, 52), inkjet printing of CNT dispersions (53, 54), screen printing of CNT dispersions (55, 56), and roll-to-roll printing of CNT dispersions (57-59), but our findings in this study should not fundamentally change if these other techniques were used. Figure 2 shows morphological features of s-SWCNT and m-SWCNT films as observed by SEM. It can be seen that all films have a dense and entangled network of SWCNTs with similar morphology which is also confirmed by AFM analysis (Figure S6). Surfactant residues are also noticeable especially in the films made using DOC-based dispersions. The images also confirm that the structure of bulk SWCNT film is similar to a CNT network in a composite rather than individual SWCNTs dispersed in a medium (60-62).

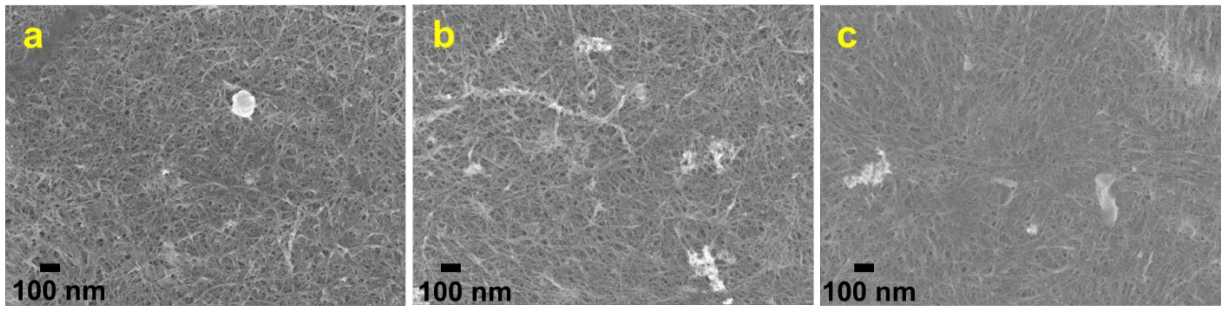

Figure 2. SEM images of 9.6 μg/cm² films of (a) s-SWCNT from DOC-based dispersion, (b) m-SWCNT from DOC-based dispersion, and (c) m-SWCNT from SDS-based dispersion.

In order to study RF heating of m- and s-SWCNT films, we used a fringing-field applicator to impose RF fields on the films. Fringing-field RF applicators provide benefits of rapid and non-contact interaction of RF electrical fields with the samples, thus making it also possible to easily apply these applicators to probe RF response of SWCNT-based electronics (63). Figure 3 shows a schematic of the fringing-field applicator. Briefly, two 13-cm long and 6-mm wide parallel copper tracks with a spacing of 2-mm were laid down on a Teflon base. RF power was supplied to the applicator via RF signal generator and a power amplifier. A Forward-Looking Infrared (FLIR) camera was used to monitor the heating response. Note that the length of the applicator is much less than the wavelength of the applied RF field; therefore, making the applicator electrically small (at 70 MHz, the wavelength is approximately 4.0 m). Due to this, the electric field is highly uniform along the copper tracks, and the applicator can be treated as a lumped circuit element instead of a transmission line with standing waves (63).

The films were placed on top of the fringing-field applicator, and 1.0 W RF power in the frequency range of 1-200 MHz was applied to determine heating rate as a function of frequency (Figure 4). The raw temporal data recorded using the FLIR camera are provided in Figures S7-S9. All films have frequency-dependent heating rates with well-defined resonant modes in the range of 60-70 MHz. At the frequency of maximum heating rates, the impedance of the RF source (50 Ω) is closely matched to the impedance due to film, applicator, and the connecting cables which leads to efficient coupling between RF energy and films (47). Note that it is also possible to induce heating in the films by using an impedance matching network and a fixed operating frequency that is within the defined industrial, scientific, and medicine (ISM) bands (47, 63). However, our data here shows that the impedance of m- and s-SWCNT films is dependent on the frequency as indicated by different heating rates.

It is seen in Figure 4 that the s-SWCNT film has higher heating rates compared to m-SWCNT films. This is primarily due to difference in DC conductivities as shown in Table 1. Since the absorbed RF energy is directly related to the electric field magnitude in the film and the electrical field magnitude is inversely proportional to the electrical conductivity of the film, the s-SWCNT film absorbs more RF energy compared to the m-SWCNT film (48, 64). The absorbed RF energy induces electric currents in the s-

SWCNT film that are more uniformly distributed than those induced in m-SWCNT films. The flow of these currents is opposed in the films due to electrical resistance caused by collisions of electrons with the neighboring atoms or molecules; therefore, resulting in Joule heating (65). In addition, the m-SWCNT films depict a behavior similar to RF heating of bulk metals. High conductivity metals cannot couple well with RF energy and electric fields attenuate toward the interior of the material (65-68). Similarly, the RF fields are suppressed inside the high-conductivity m-SWCNT films which lead to induced currents that are non-uniformly distributed, with higher concentrations around the edges; therefore, resulting in overall lower heating rates (Figure S10).

It is also interesting to note that even though s-SWCNT films heat up more than m-SWCNT films at a given RF power, this is not true when individual SWCNTs are dispersed in a dielectric medium such as a surfactant solution. Figure S11 shows that the m-SWCNT dispersion heats up faster compared to the s-SWCNT dispersion. This is because when SWCNTs are dispersed in a dielectric, the overall conductivity, or loss tangent, of the SWCNT dispersion is higher than that of the dielectric alone (which is extremely small compared to SWCNTs). Small amount of high-conductivity m-SWCNTs results in a dispersion with higher loss tangent than that of large amount of low-conductivity s-SWCNTs, which leads to overall higher heating of m-SWCNT dispersion (65, 69).

In Figure 4, we also notice that the m-SWCNT film made using DOC-based dispersion has higher heating rates compared to the film made using SDS-based dispersion. This is also correlated with DC conductivity differences as given in Table 1. The difference in conductivities of m-SWCNT films is due to presence of residual surfactant and s-SWCNT impurities especially in the film made using DOC-based dispersion. The DOC is not easily washed away compared to SDS during vacuum filtration of dispersions because of its high strength of interaction with SWCNTs. This residual DOC creates high resistance barriers at the inter-SWCNT junctions which lowers the conductivity of the film (70, 71). Additionally, the low-conductivity s-SWCNT impurities further contributes to decreasing the overall conductivity of the film. These observations show that it is also possible to use RF heating as a metric for m-SWCNT film purity. The presence of DOC and s-SWCNT impurities decrease the conductivity of the film and this leads to higher RF heating rate, whereas, a relatively pure and high-conductivity m-SWCNT film from SDS-based dispersion show very small RF heating rates.

It should be noted that the actual conductivity of m- or s-SWCNTs and their films may vary based on differences in synthesis procedures (resulting in varying defect density or chiral distribution). Nevertheless, our data here shows that regardless of the source, the bulk DC conductivity of the film scales inversely with RF heating rate (Table 1, Figure S12). Of course, at low areal density, this relationship would not hold. We observed a similar behavior for MWCNT-PLA composite films in our earlier work on welding of 3D-printed parts by locally-induced microwave heating (48). The transmitted,

reflected, and dissipated power at the films were measured and correlated with the heating response during 2.45 GHz microwave exposure of various powers. It was determined that higher CNT loadings increased the overall DC conductivity of films (68, 72), which subsequently decreased the dissipated power at the films and increased the reflected power. Since heating is primarily due to the dissipated power, it can be concluded that the microwave heating rate decreases with increase in conductivity. However, this was not true at lower CNT loadings (48). Here, we confirm that this non-monotonic relationship also holds for low frequency RF heating of CNT-based materials.

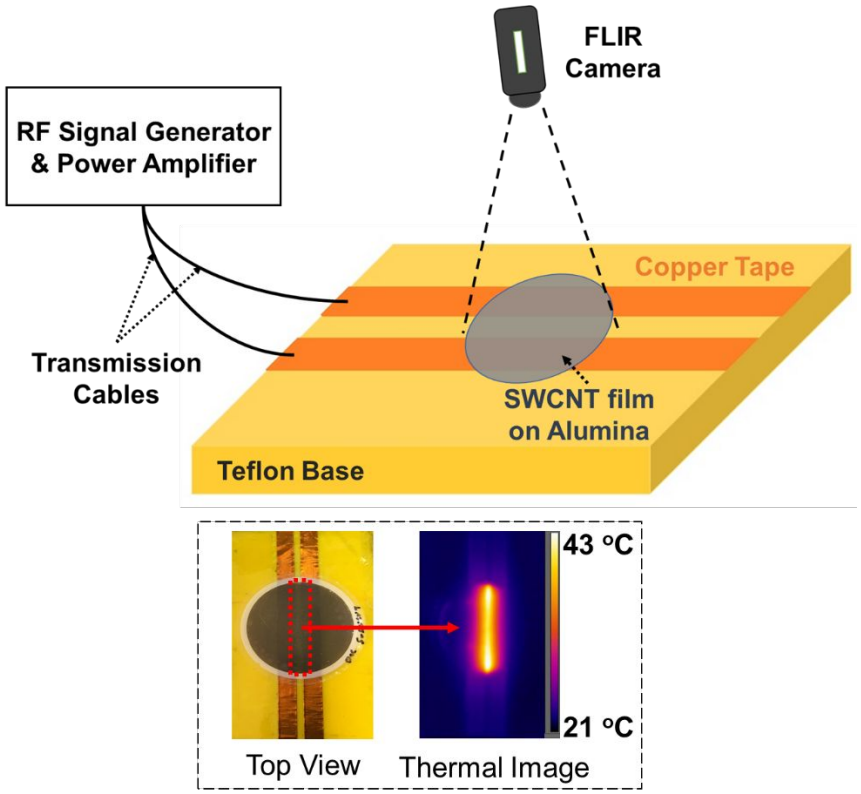

Figure 3. Schematic of the fringing-field RF applicator for heating SWCNT films. Note that alumina is non-conductive and inert to RF fields.

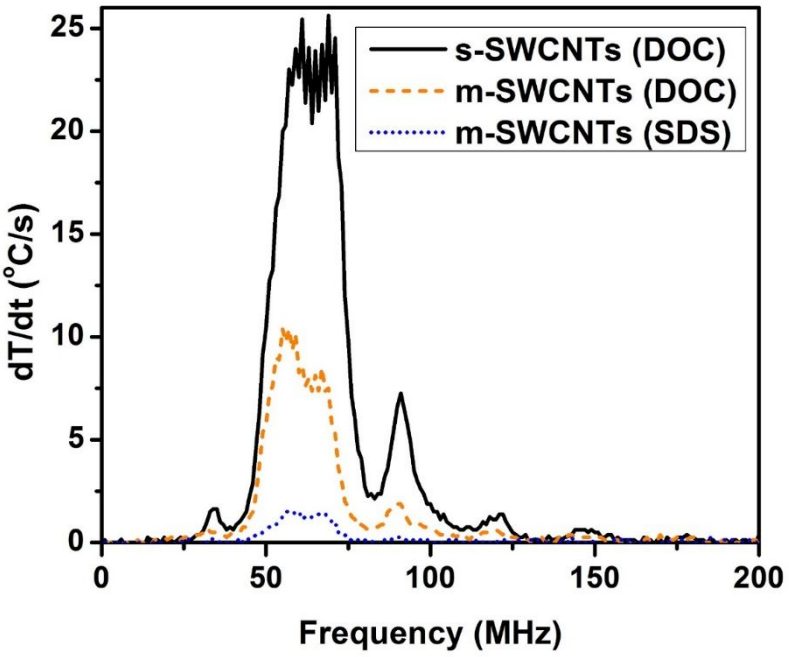

Figure 4. Heating rate, dT/dt, as a function of radio frequency for s-SWCNT film from DOC-based dispersion and m-SWCNT films from DOC-and SDS-based dispersions. Films were heated using 1.0 W RF power.

Table 1. DC conductivity and maximum RF heating rate of m- and s-SWCNT films.

	DC Conductivity	Maximum Heating Rate at 1.0 W
Film	**S/m**	**˚C/s**
s-SWCNT*	7,800	25.6
m-SWCNT*	22,700	10.4
m-SWCNT**	49,000	1.51

*From DOC-based dispersion, **From SDS-based dispersion.

Figures 5a-c show maximum temperature as a function of time for s-SWCNT and m-SWCNT films at different RF powers and a frequency of 70 MHz. The temperature increases with power for all films with s-SWCNT film heating more than 120 °C in less than 5 s at a power of 3.2 W. These tests show that each system reaches thermal equilibrium as the generated heat is balanced by convective losses to the environment. The relationship between the heating rate and power is determined to be directly proportional across all samples as seen in Figure 5d.

The high RF heating rates observed especially for s-SWCNT films is a matter of concern when applied to SWCNT-based electronics. It is because Joule heating has

been shown to affect *I-V* characteristics, signal delay, output conductance, and current densities in graphene and s-SWCNT transistors; thus, affecting their overall performance (73, 74). Additionally, the s-SWCNT films have also attracted tremendous interest as components of RF electronics such as transistors, antennas, amplifiers, and mixers (44, 75, 76). Since these devices utilize radio frequencies in the commercially relevant range of 40 MHz - 25 GHz, we anticipate that RF heating may occur in these devices and heat rates as high as 80 °C/s would decrease their performance and lifetime (44, 76-78).

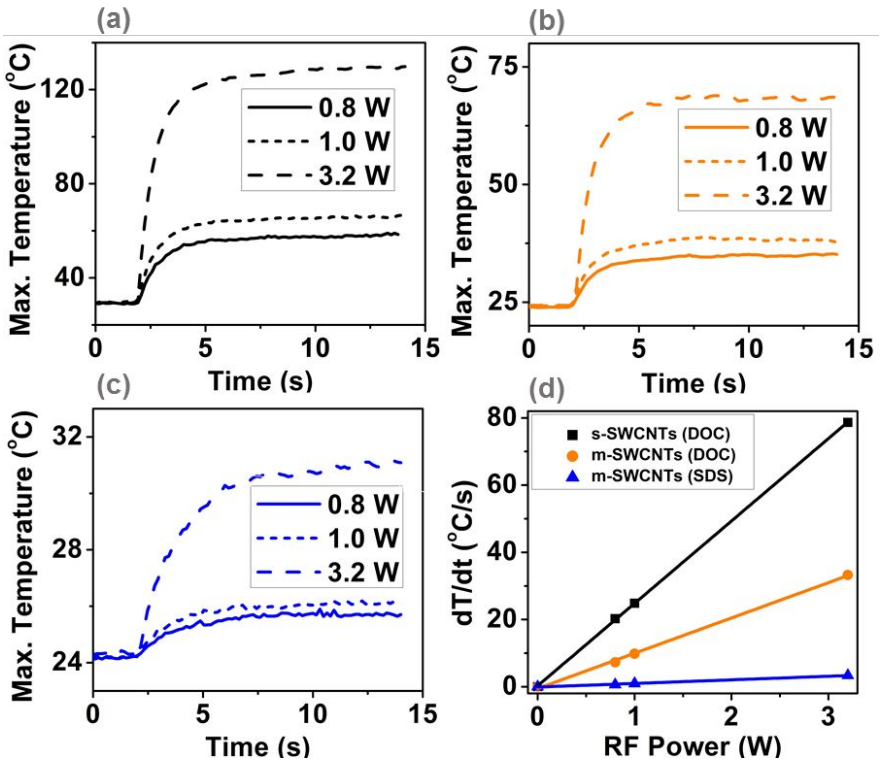

Figure 5. (a)-(c) Maximum temperature as a function of time for s-SWCNT film from DOC-based dispersion, m-SWCNT film from DOC-based dispersion, and m-SWCNT film from SDS-based dispersion, respectively. (d) Heating rate as a function of RF power for all films. Films were heated using 70 MHz RF fringing-fields at all powers.

Conclusions

We investigated the interaction of electric fields at RF frequencies with m- and s-SWCNT films using a fringing-field applicator. We observed Joule heating in all films with m-SWCNT films heating at a much lower rate compared to s-SWCNT films. We also confirmed the complex non-monotonic relationship between RF heating rate and conductivity for CNT-based materials. Our results help in understanding the contributions to RF field interactions of metallic and semiconducting shells in MWCNTs. Additionally, based on our findings, we anticipate that RF heating may occur in SWCNT-

based electronic devices and affect their performance and lifetime. Lastly, since impurities in the films affect the conductivity and thus RF heating rate, it is also possible to use RF heating as a metric for film purity.

Experimental

Materials

Nanopure water (18 mΩ) was used in all experiments. Sodium dodecyl sulfate (SDS) (≥ 99%) and sodium deoxycholate (DOC) (≥ 97%) were purchased from Sigma-Aldrich and used as received. HiPCO SWCNTs were obtained from NanoIntegris (HR25-042) and used as received. The hydrogel (Sepharose 6FF) was manufactured by GE Healthcare and purchased directly from GE.

Initial SWCNT dispersion

Raw SWCNT powder weighing 40 mg was added to 150 mL of 35.0 mM SDS solution and mixed at 8000 rpm (IKA T-25 Ultra-Turrax) for 40 min. After homogenization, the solution was allowed to rest for 15 min and then cup horn ultra-sonication (120 W, Misonix S3000) was applied to aid dispersion. The ultra-sonication step was repeated a total of three times (10 min each) to ensure a well-mixed dispersion. Finally, the dispersion was ultra-centrifuged (Beckman Coulter Optima L-80K, SW-28 rotor) for 4 h at 20,000 rpm (53,000g) to remove metallic catalysts, amorphous carbon, and SWCNT bundles from aqueous solution.

Column separation of m- and s-SWCNTs

The single column chromatography experiments were completely automated (Chromeleon software), allowing for coordinated elution gradients and real-time fraction characterization using a spectrophotometer. Sample injection and the elution were controlled by a HPLC pump (Ultimate 3000, Dionex). The low-pressure chromatography column (Bio-Rad) was made of glass and had an inner diameter of 1.5 cm. The column was packed with a hydrogel and connected to the HPLC pump using a flow adaptor. Sepharose 6FF hydrogel was selected for its high-throughput and high-purity separation of SWCNTs. The column and eluents were submerged in a water bath and chilled to 10°C. The flow rate was set at 1 mL/min and the column was packed with 5.0 mL of Sepharose 6FF, resulting in a column height of 3.0 cm. After packing with hydrogel, column was stabilized with 4 column volumes (CVs) of 35.0 mM SDS solution. SWCNT dispersion measuring 1 mL (20% CV) was injected into the column and m-SWCNT portion of the injected sample was collected through elution with SDS solution. The

separation was repeated 16 times for the collection of 5.10 ppm m-SWCNTs dispersed in SDS solution. Surfactant change process was then carried out from SDS to DOC using a 10 mL filtration cell with 100 kDa membrane (Millipore Sigma). The separation was repeated 25 times for the collection of 2.71 ppm m-SWCNTs dispersed in DOC solution (Note that the concentration is lower than 5.10 ppm due to mass loss during surfactant exchange process). The remaining SWCNTs (s-SWCNTs) were collected after the introduction of 3 CVs of a 24.4 mM DOC solution. The separation was repeated 32 times for the collection of 11.74 ppm s-SWCNTs dispersed in DOC solution. These concentrated fractions of m-SWCNTs and s-SWCNTs were characterized by absorbance and fluorescence spectroscopy, as described below.

Vacuum filtration

Appropriate volumes of 2.71 ppm m-SWCNTs and 11.74 ppm s-SWCNTs dispersed in DOC solution, and 5.10 ppm m-SWCNTs dispersed in SDS solution were vacuum filtered using a 0.1 μm pore size and 60 μm thick alumina membrane (Whatman). After the dispersions were filtered, the vacuum was kept on for ~30 min to make sure that the film is mostly dried. Distilled water was used to wash away the residual surfactant left in the film. Washing was continued until the initial soap bubbles laden permeate stream became water clear in the vacuum funnel.

SWCNTs characterization

The separated m-SWCNTs and s-SWCNTs fractions were characterized by absorption (1.0 cm path) and fluorescence (1.0 cm path) spectroscopy on an Applied NanoFluorescence Nanospectralyzer (Houston, TX) with excitation from 662 nm diode lasers. Spectra were normalized using absorbance at wavelength of 626 nm. The size (diameter) distribution was obtained after analysis using the Applied NanoFluorescence software. Multimode scanning probe microscope (AFM) (Bruker Dimension Icon) operated in a tapping mode and a scanning electron microscope (SEM) (JEOL JSM-7500F instrument) at 2 kV accelerating voltage was used to determine film thickness and morphological features of vacuum filtered films of m-SWCNTs and s-SWCNTs. Four-point probe was used to measure resistivity of films and DC conductivity was calculated as a reciprocal of resistivity.

RF heating of films

A fringing-field capacitor was fabricated using two parallel 13 cm long copper tracks with a spacing of 2 mm. The samples, m-SWCNT and s-SWCNT films on alumina membrane, were placed on top of the capacitor. A signal generator (Rigol Inc., DSG815) and a 500 W amplifier (Prana R&D, GN500D) were used to supply RF power to the capacitor. The capacitor was connected to the amplifier with a 50 Ω coaxial transmission line terminated by a type N bulkhead connector with alligator clips soldered to the center pin and ground reference. FLIR infrared camera (FLIR Systems Inc., A655sc) was used to monitor heating of films over time, and to generate temporal plots. In order to obtain the frequency-dependent heating response of the films, a step-

wise heat-cool frequency sweep was programmed into the signal generator. Frequencies from 1 to 200 MHz were swept such that power at 1.0 W is applied for 1 s, followed by 13 s of cooling before moving to the next 1 MHz incremental step. The heating rates as a function of frequency were determined by selecting the points when the power is switched on and ~0.8 s into each cycle and calculating the slope between the points. The raw temperature vs. time data are provided in Figures S7-S9.

Conflicts of Interest

There are no conflicts to declare.

Acknowledgements

We acknowledge helpful advice from V.K. Hicks, E.B. Porter, N. Patil of TAMU and C. B. Sweeney of Essentium 3D. We also acknowledge Materials Characterization Facility (MCF) at TAMU for help with SWCNT characterization. We also acknowledge funding from the U.S. Army Engineer Research and Development Center (ERDC) under cooperative agreement W912HZ-17-2-0007.

References

1. Lee WJ, Clancy AJ, Fernández-Toribio JC, Anthony DB, White ER, Solano E, et al. Interfacially-grafted single-walled carbon nanotube / poly (vinyl alcohol) composite fibers. Carbon. 2019;146:162-71.
2. Gu H, Zhang H, Ma C, Xu X, Wang Y, Wang Z, et al. Trace electrosprayed nanopolystyrene facilitated dispersion of multiwalled carbon nanotubes: Simultaneously strengthening and toughening epoxy. Carbon. 2019;142:131-40.
3. Simon P, Gogotsi Y. Materials for electrochemical capacitors. Nature Materials. 2008;7:845.
4. Simon P, Gogotsi Y. Capacitive Energy Storage in Nanostructured Carbon–Electrolyte Systems. Accounts of Chemical Research. 2013;46(5):1094-103.
5. Hummer G, Rasaiah JC, Noworyta JP. Water conduction through the hydrophobic channel of a carbon nanotube. Nature. 2001;414(6860):188-90.
6. Kalra A, Garde S, Hummer G. Osmotic water transport through carbon nanotube membranes. Proceedings of the National Academy of Sciences. 2003;100(18):10175.
7. De Volder MFL, Tawfick SH, Baughman RH, Hart AJ. Carbon Nanotubes: Present and Future Commercial Applications. Science. 2013;339(6119):535.
8. Luo X, Weng W, Liang Y, Hu Z, Zhang Y, Yang J, et al. Multifunctional fabrics of carbon nanotube fibers. Journal of Materials Chemistry A. 2019;7(15):8790-7.
9. Park S, Vosguerichian M, Bao Z. A review of fabrication and applications of carbon nanotube film-based flexible electronics. Nanoscale. 2013;5(5):1727-52.
10. Lipomi DJ, Vosgueritchian M, Tee BCK, Hellstrom SL, Lee JA, Fox CH, et al. Skin-like pressure and strain sensors based on transparent elastic films of carbon nanotubes. Nat Nanotechnol. 2011;6:788.
11. Rao R, Pint CL, Islam AE, Weatherup RS, Hofmann S, Meshot ER, et al. Carbon Nanotubes and Related Nanomaterials: Critical Advances and Challenges for Synthesis toward Mainstream Commercial Applications. Acs Nano. 2018;12(12):11756-84.
12. Avouris P, Appenzeller J, Martel R, Wind SJ. Carbon nanotube electronics. Proceedings of the IEEE. 2003;91(11):1772-84.
13. Qiu C, Zhang Z, Xiao M, Yang Y, Zhong D, Peng L-M. Scaling carbon nanotube complementary transistors to 5-nm gate lengths. Science. 2017;355(6322):271.
14. Rao SG, Huang L, Setyawan W, Hong S. Large-scale assembly of carbon nanotubes. Nature. 2003;425:36.
15. Avouris P. Molecular Electronics with Carbon Nanotubes. Accounts of Chemical Research. 2002;35(12):1026-34.
16. Geim AK, Novoselov KS. The rise of graphene. Nature Materials. 2007;6:183.
17. Weisman RB, Bachilo SM. Dependence of Optical Transition Energies on Structure for Single-Walled Carbon Nanotubes in Aqueous Suspension: An Empirical Kataura Plot. Nano Lett. 2003;3(9):1235-8.
18. Hamada N, Sawada S-i, Oshiyama A. New one-dimensional conductors: Graphitic microtubules. Phys Rev Lett. 1992;68(10):1579-81.
19. Zhao Y, Clar JG, Li LP, Xu J, Yuan TY, Bonzongo JCJ, et al. Selective desorption of high-purity (6,5) SWCNTs from hydrogels through surfactant modulation. Chem Commun. 2016;52(14):2928-31.

20. Arnold MS, Green AA, Hulvat JF, Stupp SI, Hersam MC. Sorting carbon nanotubes by electronic structure using density differentiation. Nat Nanotechnol. 2006;1:60.
21. Ihara K, Endoh H, Saito T, Nihey F. Separation of Metallic and Semiconducting Single-Wall Carbon Nanotube Solution by Vertical Electric Field. The Journal of Physical Chemistry C. 2011;115(46):22827-32.
22. Liu H, Nishide D, Tanaka T, Kataura H. Large-scale single-chirality separation of single-wall carbon nanotubes by simple gel chromatography. Nature Communications. 2011;2:309.
23. Bradley K, Gabriel J-CP, Grüner G. Flexible Nanotube Electronics. Nano Letters. 2003;3(10):1353-5.
24. Tang J, Cao Q, Tulevski G, Jenkins KA, Nela L, Farmer DB, et al. Flexible CMOS integrated circuits based on carbon nanotubes with sub-10 ns stage delays. Nature Electronics. 2018;1(3):191-6.
25. Yao Z, Kane CL, Dekker C. High-Field Electrical Transport in Single-Wall Carbon Nanotubes. Phys Rev Lett. 2000;84(13):2941-4.
26. Zaumseil J. Single-walled carbon nanotube networks for flexible and printed electronics. Semicond Sci Tech. 2015;30(7).
27. Cao Q, Tersoff J, Farmer DB, Zhu Y, Han S-J. Carbon nanotube transistors scaled to a 40-nanometer footprint. Science. 2017;356(6345):1369.
28. Kong J, Franklin NR, Zhou C, Chapline MG, Peng S, Cho K, et al. Nanotube Molecular Wires as Chemical Sensors. Science. 2000;287(5453):622.
29. Liu L, Ding L, Zhong D, Han J, Wang S, Meng Q, et al. Carbon Nanotube Complementary Gigahertz Integrated Circuits and Their Applications on Wireless Sensor Interface Systems. Acs Nano. 2019;13(2):2526-35.
30. Zhang H, Xiang L, Yang Y, Xiao M, Han J, Ding L, et al. High-Performance Carbon Nanotube Complementary Electronics and Integrated Sensor Systems on Ultrathin Plastic Foil. Acs Nano. 2018;12(3):2773-9.
31. Snow ES, Novak JP, Campbell PM, Park D. Random networks of carbon nanotubes as an electronic material. Appl Phys Lett. 2003;82(13):2145-7.
32. Kocabas C, Hur S-H, Gaur A, Meitl MA, Shim M, Rogers JA. Guided Growth of Large-Scale, Horizontally Aligned Arrays of Single-Walled Carbon Nanotubes and Their Use in Thin-Film Transistors. Small. 2005;1(11):1110-6.
33. Zhao C, Zhong D, Han J, Liu L, Zhang Z, Peng L-M. Exploring the Performance Limit of Carbon Nanotube Network Film Field-Effect Transistors for Digital Integrated Circuit Applications. Advanced Functional Materials. 2019;0(0):1808574.
34. Menon H, Aiswarya R, Surendran KP. Screen printable MWCNT inks for printed electronics. RSC Advances. 2017;7(70):44076-81.
35. Noyce SG, Doherty JL, Cheng Z, Han H, Bowen S, Franklin AD. Electronic Stability of Carbon Nanotube Transistors Under Long-Term Bias Stress. Nano Lett. 2019.
36. Avery AD, Zhou BH, Lee J, Lee ES, Miller EM, Ihly R, et al. Tailored semiconducting carbon nanotube networks with enhanced thermoelectric properties. Nat Energy. 2016;1.

37. Javey A, Guo J, Farmer DB, Wang Q, Wang D, Gordon RG, et al. Carbon Nanotube Field-Effect Transistors with Integrated Ohmic Contacts and High-κ Gate Dielectrics. Nano Lett. 2004;4(3):447-50.
38. Cao Y, Che Y, Seo J-WT, Gui H, Hersam MC, Zhou C. High-performance radio frequency transistors based on diameter-separated semiconducting carbon nanotubes. Appl Phys Lett. 2016;108(23):233105.
39. Zhang DH, Ryu K, Liu XL, Polikarpov E, Ly J, Tompson ME, et al. Transparent, conductive, and flexible carbon nanotube films and their application in organic light-emitting diodes. Nano Lett. 2006;6(9):1880-6.
40. Guillot SL, Mistry KS, Avery AD, Richard J, Dowgiallo A-M, Ndione PF, et al. Precision printing and optical modeling of ultrathin SWCNT/C60 heterojunction solar cells. Nanoscale. 2015;7(15):6556-66.
41. Green AA, Hersam MC. Colored Semitransparent Conductive Coatings Consisting of Monodisperse Metallic Single-Walled Carbon Nanotubes. Nano Lett. 2008;8(5):1417-22.
42. Miyata Y, Yanagi K, Maniwa Y, Kataura H. Highly stabilized conductivity of metallic single wall carbon nanotube thin films. J Phys Chem C. 2008;112(10):3591-6.
43. Schindler A, Brill J, Fruehauf N, Novak JP, Yaniv Z. Solution-deposited carbon nanotube layers for flexible display applications. Physica E: Low-dimensional Systems and Nanostructures. 2007;37(1):119-23.
44. Kocabas C, Kim H-s, Banks T, Rogers JA, Pesetski AA, Baumgardner JE, et al. Radio frequency analog electronics based on carbon nanotube transistors. Proceedings of the National Academy of Sciences. 2008;105(5):1405.
45. Gannon CJ, Cherukuri P, Yakobson BI, Cognet L, Kanzius JS, Kittrell C, et al. Carbon nanotube-enhanced thermal destruction of cancer cells in a noninvasive radiofrequency field. Cancer-Am Cancer Soc. 2007;110(12):2654-65.
46. Corr SJ, Raoof M, Cisneros BT, Orbaek AW, Cheney MA, Law JJ, et al. Radiofrequency electric-field heating behaviors of highly enriched semiconducting and metallic single-walled carbon nanotubes. Nano Res. 2015;8(9):2859-70.
47. Sweeney CB, Moran AG, Gruener JT, Strasser AM, Pospisil MJ, Saed MA, et al. Radio Frequency Heating of Carbon Nanotube Composite Materials. Acs Applied Materials & Interfaces. 2018;10(32):27252-9.
48. Sweeney CB, Lackey BA, Pospisil MJ, Achee TC, Hicks VK, Moran AG, et al. Welding of 3D-printed carbon nanotube-polymer composites by locally induced microwave heating. Sci Adv. 2017;3(6).
49. Bachilo SM, Strano MS, Kittrell C, Hauge RH, Smalley RE, Weisman RB. Structure-Assigned Optical Spectra of Single-Walled Carbon Nanotubes. Science. 2002;298(5602):2361.
50. Clar JG, Yuan T, Zhao Y, Bonzongo J-CJ, Ziegler KJ. Evaluation of Critical Parameters in the Separation of Single-Wall Carbon Nanotubes through Selective Adsorption onto Hydrogels. The Journal of Physical Chemistry C. 2014;118(28):15495-505.
51. Silvera-Batista CA, Scott DC, McLeod SM, Ziegler KJ. A Mechanistic Study of the Selective Retention of SDS-Suspended Single-Wall Carbon Nanotubes on Agarose Gels. The Journal of Physical Chemistry C. 2011;115(19):9361-9.

52. Tenent RC, Barnes TM, Bergeson JD, Ferguson AJ, To B, Gedvilas LM, et al. Ultrasmooth, Large-Area, High-Uniformity, Conductive Transparent Single-Walled-Carbon-Nanotube Films for Photovoltaics Produced by Ultrasonic Spraying. Adv Mater. 2009;21(31):3210-+.
53. Okimoto H, Takenobu T, Yanagi K, Miyata Y, Shimotani H, Kataura H, et al. Tunable Carbon Nanotube Thin-Film Transistors Produced Exclusively via Inkjet Printing. Adv Mater. 2010;22(36):3981-6.
54. Subbaraman H, Pham DT, Xu X, Chen MY, Hosseini A, Lu X, et al. Inkjet-Printed Two-Dimensional Phased-Array Antenna on a Flexible Substrate. IEEE Antennas and Wireless Propagation Letters. 2013;12:170-3.
55. Cao X, Chen H, Gu X, Liu B, Wang W, Cao Y, et al. Screen Printing as a Scalable and Low-Cost Approach for Rigid and Flexible Thin-Film Transistors Using Separated Carbon Nanotubes. Acs Nano. 2014;8(12):12769-76.
56. Shi YS, Zhu C-C, Qikun W, Xin L. Large area screen-printing cathode of CNT for FED. Diamond and Related Materials. 2003;12(9):1449-52.
57. Lee W, Koo H, Sun J, Noh J, Kwon K-S, Yeom C, et al. A fully roll-to-roll gravure-printed carbon nanotube-based active matrix for multi-touch sensors. Sci Rep-Uk. 2015;5:17707.
58. Fischer T, Rühling J, Wetzold N, Zillger T, Weissbach T, Göschel T, et al. Roll-to-roll printed carbon nanotubes on textile substrates as a heating layer in fiber-reinforced epoxy composites. Journal of Applied Polymer Science. 2018;135(10):45950.
59. Zhou B, Li Y, Zheng G, Dai K, Liu C, Ma Y, et al. Continuously fabricated transparent conductive polycarbonate/carbon nanotube nanocomposite films for switchable thermochromic applications. J Mater Chem C. 2018;6(31):8360-71.
60. Che J, Chen P, Chan-Park MB. High-strength carbon nanotube buckypaper composites as applied to free-standing electrodes for supercapacitors. Journal of Materials Chemistry A. 2013;1(12):4057-66.
61. Jin Gyu P, Jeffrey L, Qunfeng C, Jianwen B, Jesse S, Richard L, et al. Electromagnetic interference shielding properties of carbon nanotube buckypaper composites. Nanotechnology. 2009;20(41):415702.
62. Du F, Scogna RC, Zhou W, Brand S, Fischer JE, Winey KI. Nanotube Networks in Polymer Nanocomposites: Rheology and Electrical Conductivity. Macromolecules. 2004;37(24):9048-55.
63. Mehdizadeh M. Microwave/RF Applicators and Probes for Material Heating, Sensing, and Plasma Generation: William Andrew; 2009.
64. Electrical Conductivity Basics: Radio-Electronics.com; [Available from: https://radio-electronics.com/info//formulae/resistance/electrical-conductivity.php.
65. Sun J, Wang W, Yue Q. Review on Microwave-Matter Interaction Fundamentals and Efficient Microwave-Associated Heating Strategies. Materials (Basel, Switzerland). 2016;9(4):231.
66. Yoshikawa N. Fundamentals and Applications of Microwave Heating of Metals. Journal of Microwave Power and Electromagnetic Energy. 2010;44(1):4-13.
67. Rybakov KI, Semenov VE, Egorov SV, Eremeev AG, Plotnikov IV, Bykov YV. Microwave heating of conductive powder materials. J Appl Phys. 2006;99(2):023506.

68. Cheng C, Fan R, Ren Y, Ding T, Qian L, Guo J, et al. Radio frequency negative permittivity in random carbon nanotubes/alumina nanocomposites. Nanoscale. 2017;9(18):5779-87.
69. Sillars RW. The properties of a dielectric containing semiconducting particles of various shapes. Institution of Electrical Engineers - Proceedings of the Wireless Section of the Institution. 1937;12(35):139-55.
70. Zeng X, Yang D, Liu H, Zhou N, Wang Y, Zhou W, et al. Detecting and Tuning the Interactions between Surfactants and Carbon Nanotubes for Their High-Efficiency Structure Separation. Advanced Materials Interfaces. 2018;5(2):1700727.
71. Bekyarova E, Itkis ME, Cabrera N, Zhao B, Yu AP, Gao JB, et al. Electronic properties of single-walled carbon nanotube networks. J Am Chem Soc. 2005;127(16):5990-5.
72. Hu C, Li Z, Wang Y, Gao J, Dai K, Zheng G, et al. Comparative assessment of the strain-sensing behaviors of polylactic acid nanocomposites: reduced graphene oxide or carbon nanotubes. J Mater Chem C. 2017;5(9):2318-28.
73. Islam S, Li Z, Dorgan VE, Bae M, Pop E. Role of Joule Heating on Current Saturation and Transient Behavior of Graphene Transistors. Ieee Electr Device L. 2013;34(2):166-8.
74. Xing C, Yin W, Liu L, Huang J. Investigation on Self-Heating Effect in Carbon Nanotube Field-Effect Transistors. Ieee T Electron Dev. 2011;58(2):523-9.
75. Rutherglen C, Jain D, Burke P. Nanotube electronics for radiofrequency applications. Nat Nanotechnol. 2009;4(12):811-9.
76. Jensen K, Weldon J, Garcia H, Zettl A. Nanotube Radio. Nano Lett. 2007;7(11):3508-11.
77. Shoucair FS. Potential and problems of high-temperature electronics and CMOS integrated circuits (25–250°C) - an overview. Microelectronics Journal. 1991;22(2):39-54.
78. Schroder DK, Babcock JA. Negative bias temperature instability: Road to cross in deep submicron silicon semiconductor manufacturing. J Appl Phys. 2003;94(1):1-18.

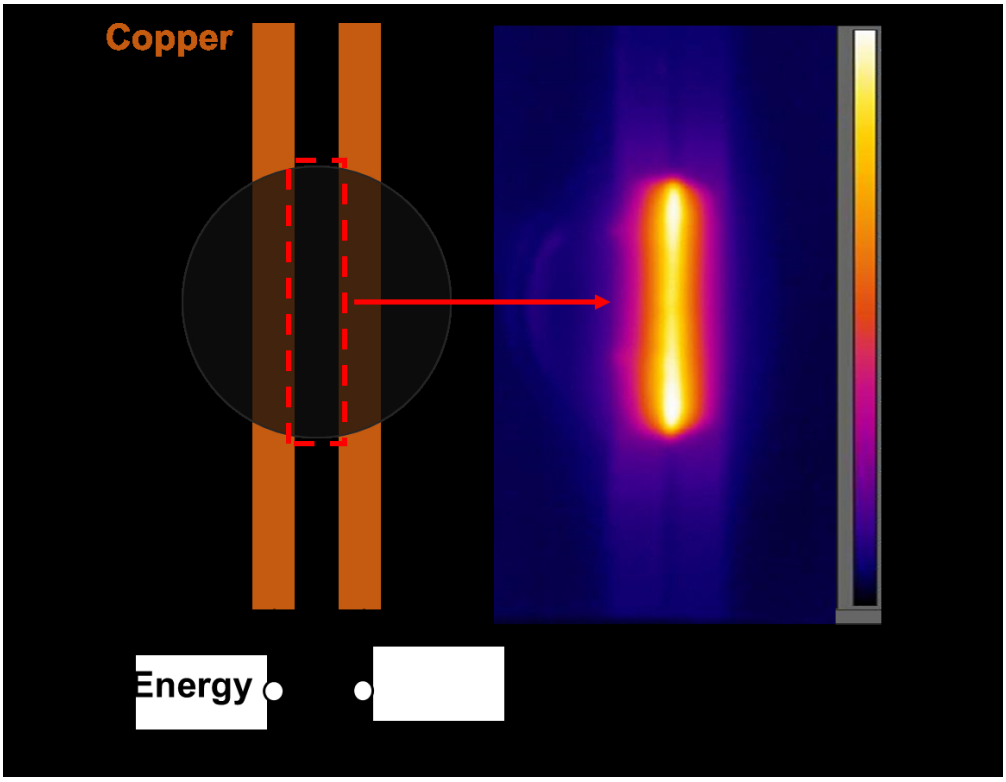
Copper
Energy